Appl. Phys. B 75, 771–778 (2002)
DOI: 10.1007/s00340-002-1020-7

Applied Physics B
Lasers and Optics

M. AFZELIUS[1,3,✉]
P.-E. BENGTSSON[1]
J. BOOD[2]
J. BONAMY[3]
F. CHAUSSARD[4]
H. BERGER[4]
T. DREIER[5]

Dual-broadband rotational CARS modelling of nitrogen at pressures up to 9 MPa. II. Rotational Raman line widths

[1] Department of Combustion Physics, Lund Institute of Technology, P.O. Box 118, 22100 Lund, Sweden
[2] Combustion Research Facility, Sandia National Laboratories, MS 9055, P.O. Box 969, Livermore, CA 94551, USA
[3] Laboratoire de Physique Moléculaire, UMR CNRS 6624, Université de Franche-Comté, La Bouloie, 25030 Besançon cedex, France
[4] Laboratoire de Physique, UMR CNRS 5027, Université de Bourgogne, BP 47870, 21078 Dijon cedex, France
[5] Institut für Technische Verbrennung, Pfaffenwaldring 12, 70569 Stuttgart, Germany

Received: 18 February 2002/Revised version: 9 July 2002
Published online: 22 November 2002 •

ABSTRACT Rotational coherent anti-Stokes Raman spectroscopy (CARS) is a well-established spectroscopic technique for thermometry at pre-combustion temperatures and atmospheric pressure. However, at pressures of several MPa, a previous investigation revealed large discrepancies between experimental data and the theoretical model. A re-evaluation has been made of these data (at room temperature and in the range 1.5–9 MPa) with two improvements to the spectral code. The first is the inclusion of an inter-branch interference effect, which is described in detail in Paper I. The second is the use of experimental S_1-branch Raman line widths measured at 295 K, with a temperature dependence extracted from semi-classical calculations following the Robert–Bonamy formalism. It is shown that these two modifications significantly improve the theoretical model, since both the spectral fits and the accuracy of the evaluated temperatures are considerably improved.

PACS 42.65.Dr; 33.70.Jg

1 Introduction

Rotational coherent anti-Stokes Raman spectroscopy (CARS) has since the beginning of the 1980s proven to be an accurate method for gas thermometry at atmospheric pressure, especially in nitrogen in the range 135–1500 K [1–4], and in air in the range 300–2000 K [5, 6]. It is thus not surprising that rotational CARS has been used for combustion diagnostics, since in air-fed premixed combustion the nitrogen concentration is high at all times, from unburned mixture to product gas.

In normal combustion situations the range of temperature spans from room temperature to flame temperatures. However, it is well known that the accuracy of rotational CARS thermometry gradually decreases with increasing temperature [2, 4]. The main reason for this feature is that the shape of a rotational CARS spectrum changes noticeably in the lower-temperature range, which can be related to the Boltzmann population distribution over rotational energy levels in the vibrational ground state at different temperatures. Since this Boltzmann distribution is well known, there is no uncertainty related to this parameter. The second most important parameter for the temperature sensitivity of the spectral shape is the Raman line widths, which in addition to their inherent temperature dependence also have a rotational J-quantum number dependence. Consequently, the intensity of the individual lines is affected and subsequently also the evaluated temperature.

The Raman lines of nitrogen are nearly purely pressure-broadened in the considered pressure region (above ambient pressure), and thus they result from molecular collisions. Although Raman-broadening coefficients can be calculated within semi-classical frameworks [7–9] developed for pressure-broadened spectral lines, they have a limited accuracy even for key species such as N_2 and O_2 due to the lack of precise energy-potential surfaces, especially for close collisions. Instead, one usually has to rely on dynamical scaling laws, like the ECS [10] (energy-corrected sudden) and MEG [11] (modified exponential gap) laws that are fitted to experimental data. Unfortunately, the temperature and J-dependence of pure rotational Raman line widths have not been experimentally well studied, as opposed to vibrational Q-branch line widths, and some inaccuracy in the evaluated temperature due to uncertainties in line-width data must be expected.

For atmospheric pressure and room-temperature conditions, the lines in a rotational CARS spectrum are well resolved, and the evaluated temperature is not strongly correlated to the value of the non-resonant susceptibility. This implies that small uncertainties in this parameter do not influence the evaluated temperatures. Therefore, it is not surprising that rotational CARS thermometry has been shown to be successful at these conditions [3]. However, as pressure increases further, the characteristics of the rotational CARS spectrum change. The individual lines are broadened, and the influence of the non-resonant susceptibility on the spectral shape increases. Further, since the line widths scale linearly with pressure, the absolute error related to these will also increase linearly. Consequently, the accuracy of the Raman line widths will be more crucial for a good temperature evaluation. Yet, we will demonstrate in this article that this feature can be

✉ Fax: +46-46/2224542, E-mail: mikael.afzelius@forbrf.lth.se

used to test different line-width models, since both spectral fit and evaluated temperature are more sensitive to the different models at evaluated pressure.

The purpose of this paper is to report a re-evaluation of rotational CARS spectra recorded at room temperature and in a large pressure range [12], using a modified rotational CARS code. The first evaluation of these spectra revealed deficiencies in the model for rotational CARS spectra at high pressures. The difference between best-fitted and experimental spectra was large above 2 MPa and the evaluated temperature had an error of up to 25 K in the range 3–9 MPa.

Therefore, we have further developed our model for spectral calculation by two modifications. Firstly, we have considered the effect of CSRS (coherent Stokes Raman scattering) lines on the CARS side of the spectrum. This inter-branch interference effect is explained in detail in Paper I [13]. Secondly, we have replaced our Raman line widths, previously approximated from vibrational Q-branch line widths, by rovibrational S_1-branch line widths. These new line widths are based on high-resolution Raman measurements [14–16] and semi-classical line-width calculations following the Robert–Bonamy (RB) formalism [9]. This second paper deals with the new line widths and presents the results of the re-evaluation of the data from [12].

2 Dual-broadband rotational CARS thermometry

Rotational coherent anti-Stokes Raman scattering is a third-order optical process where three laser beams interact with rotational levels in a molecule and produce a resonant coherent signal. In CARS thermometry the signal is spectrally resolved and the temperature is determined by a spectral fit to theoretically calculated spectra. To attain a high accuracy, the model for spectral calculation must be very detailed, and especially the line shape of each rotational line must be modelled correctly, as the spectral lines of a rotational spectrum are well resolved. The details of the spectral calculation of CARS spectra including the inter-branch interference are described in Paper I [13].

In rotational CARS photon pairs, ω_1 and ω_2, coherently excite the molecule from level J to $J+2$, providing that $\omega_1 - \omega_2$ is equal to the frequency difference between the levels. A third photon, ω_3, scatters off this excited molecule and is anti-Stokes-shifted by the same frequency difference. Conversely, in rotational CSRS, the molecule is coherently deexcited from level $J+2$ to J, and the third photon is instead Stokes-shifted.

In the dual-broadband (DB) [17, 18] variant of rotational CARS, photons ω_1 and ω_2 are taken from the same spectrally broadband dye laser beam; thus multiple pairs of photons drive each resonance. This has several experimental advantages, among those a spectral averaging effect over the broadband dye laser profile. Another feature of the DB approach is that CARS and CSRS lines are generated simultaneously, since the difference $\omega_1 - \omega_2$ can be both positive and negative. Simultaneous CARS and CSRS generation has been studied earlier, both in the conventional approach [19, 20], and in the dual-broadband variant [18].

The total third-order susceptibility for DB rotational CARS can be written as the sum of the resonant CARS and CSRS susceptibilities and a third term representing non-resonant contributions [13]:

$$\chi^{(3)}(\omega-\omega_3) = \chi^{(3)}_{\mathrm{CARS}}(\omega-\omega_3) + \chi^{(3)}_{\mathrm{CSRS}}(\omega-\omega_3) + \chi_{nr}\,. \quad (1)$$

The resonant susceptibilities are calculated through the isolated-line approximation. The resonant CARS susceptibility can be written as a function of frequency ω [4] (throughout the paper j denotes spectral line number and J rotational quantum number):

$$\chi^{(3)}_{\mathrm{CARS}}(\omega-\omega_3) = \sum_j \frac{a_j}{\omega_j - (\omega-\omega_3) - i\Gamma_j}\,, \quad (2)$$

where

$$a_j = \frac{4}{45}\frac{N}{\hbar} b_j^{j+2} \zeta_v^2 F(j,\, j+2)\Delta\varrho_{j,\,j+2}\,, \quad (3)$$

and correspondingly for CSRS

$$\chi^{(3)}_{\mathrm{CSRS}}(\omega-\omega_3) = \sum_j \frac{c_j}{-\omega_j - (\omega-\omega_3) - i\Gamma_j}\,, \quad (4)$$

where

$$c_j = \frac{4}{45}\frac{N}{\hbar} b_{j+2}^{j} \zeta_v^2 F(j+2,\, j)\Delta\varrho_{j+2,\,j}\,, \quad (5)$$

The factors above are the following; ω_j is the rotational transition frequency for the CARS line j ($J_i = j$, $J_f = j+2$) and $-\omega_j$ is the corresponding frequency for the CSRS line j ($J_i = j+2$, $J_f = j$). Γ_j is the rotational Raman line width of line j (note that the broadening for an upward and a downward transition is the same). N is the number density, the b factor is the Placzek–Teller coefficient [21], the F factor corrects the line strength because of the centrifugal distortion [22, 23], ζ_v is the anisotropic polarisability factor [24, 25] of vibrational level v and the $\Delta\varrho$ factor is the normalised population difference between the levels.

In order to account for the finite laser line width of the pump laser and the broadband dye laser, a Kataoka–Teets convolution [26, 27] of the spectrum, over the laser-line profiles, is performed. It can be done on this modified susceptibility by writing the two resonant sums in (1) as one sum over all rotational lines and then using the standard formulas given in [4] and [13] (the first approach as explained in Paper I [13]). The final expression for the intensity can be written as:

$$I(\omega) \propto (\chi_{nr}^2 + \chi_{nr} D + E)\,, \quad (6)$$

where D and E, denoted the resonant term and the cross-term, respectively, are expressions that depend on both the CARS and CSRS resonances. At atmospheric pressure essentially only the resonant term E contributes to the intensity. However, because the three terms scale differently with pressure, the non-resonant term and the cross-term are of the same importance at higher pressures. In fact, as the pressure increases, the cross-term contracts the spectrum around the pump frequency ω_3, giving rise to the inter-branch interference effect described in Paper I [13].

The final step in building a spectrum is to convolute the intensity spectrum with a suitable instrumental function to

account for the line broadening by the spectrometer/CCD camera system. Depending on the detection system the instrumental function has a Gaussian, Lorentzian or Voigt profile.

In order to deduce the temperature from an experimental spectrum, the spectrum is fitted to a library of theoretically calculated spectra using a Levenberg–Marquardt non-linear least-squares algorithm. The spectral fit routine can simultaneously fit the temperature, the dispersion, the Raman shift of the calibration channel and the non-resonant susceptibility. However, to obtain a reliable fitting procedure at high pressures one often has to fix the dispersion when the lines start to overlap significantly, and also χ_{nr} due to its strong impact on the spectra at high pressures through the $\chi_{nr}D$ and χ_{nr}^2 factors. The minimised parameter in the non-linear least-squares fitting procedure is the sum-of-squares (SSQ):

$$SSQ = \sum_i (I_i^{\text{th}} - I_i^{\text{exp}})^2 , \tag{7}$$

where $I_i^{\text{th}}(I_i^{\text{exp}})$ is the intensity of the theoretical (experimental) spectrum at pixel i.

3 Rotational Raman line widths

In the pressure regime above atmospheric pressure, the Raman resonances are nearly purely pressure-broadened when using forward Raman scattering, the Doppler contribution being so small that it can be neglected. The line widths are thus linearly dependent on pressure for the whole range where the ideal gas law is valid, which is the case for all pressures in this study.

The Raman line widths affect the evaluated temperature through their inherent temperature dependence, but also through their J-dependence that modifies the intensity distribution over the rotational lines. Thus to determine the temperature with high accuracy, a good line-width model is crucial.

Generally, the pressure-broadened line widths in Raman and infrared spectroscopy have contributions from inelastic transfers between rotational states, re-orientational phase shifts due to collision-induced changes in the direction of the molecular axis and vibrational dephasing. The total line width can then be written in the form [28] (isotropic Q-branch, infrared P- and R-branches, and anisotropic O- and S-branches, respectively):

$$\gamma_{J_i,J_f} = \gamma_{J_i,J_f}^{\text{rot.inelastic}} + \gamma_{J_i,J_f}^{\text{reorient.}} + \gamma^{\text{vib.}},\ J_f = J_i \pm 0, 1, 2 . \tag{8}$$

Neglecting the rotation–vibration coupling, the inelastic rotational transfer is very similar in the first and second vibrational states of N_2 and the vibrational dephasing term is assumed to be independent of rotational level. The elastic vibrational contribution is only $2.8(1.6) \times 10^{-5}\ \text{cm}^{-1}\ \text{amagat}^{-1}$ at 300 K [29]. Therefore we will disregard this contribution in the following.

Pure rotational lines obviously do not have any contribution from vibrational dephasing; thus only elastic reorientation of the molecular axis and inelastic transfers between rotational levels contribute. Conversely, the broadening of isotropic Q-branch lines is independent of molecular orientation; thus the re-orientational phase shifts do not contribute to the broadening of Q-lines.

Isotropic N_2 Q-branch broadening coefficients have been well studied both experimentally [30–32] and theoretically [9, 28, 33–35] for a wide range of temperatures and rotational quantum numbers. However, there are only a few high-resolution experimental studies on pure rotational or rovibrational S-branch Raman line widths available [14–16, 36], and consequently the anisotropic re-orientational contribution to these widths is not well known. Therefore we have up to this date used broadening coefficients calculated by the random-phase approximation (RPA) [10] (9), using Q-branch isotropic line widths. The RPA assumes that the re-orientational phase shifts can be neglected, and that only inelastic collisions contribute to the broadening.

$$\gamma_{J,J+2}^{\text{RPA}} = \gamma_{J,J+2}^{\text{rot.inelastic}} = \frac{1}{2}(\gamma_{J,J} + \gamma_{J+2,J+2}) . \tag{9}$$

In Fig. 1 and Table 2, experimentally measured rovibrational S_1-branch ($\Delta\nu = 1,\ \Delta J = 2$) line widths at 295 K are compared to those calculated within the RPA approximation. The experimental line widths are a set of data from [14] measured with inverse Raman spectroscopy (IRS), and recent measurements realised in Dijon [15, 16] using a high-resolution rovibrational CARS method. Noticeably, these results are very consistent with each other. The isotropic Q-branch broadening coefficients used in the RPA have been calculated with the ECS-P scaling law using the parameters given in [4]. It should be pointed out that the ECS-P line widths fit very well to the experimental isotropic line widths [31].

The difference between the S_1 line widths and those calculated from the RPA is the contribution from re-orientational phase shifts, and as can be seen this on average constitutes approximately 10% of the total width at 295 K. It is thus well motivated to investigate how these different widths affect the temperature determination from rotational CARS spectra and, since the collision line widths scale linearly with pressure,

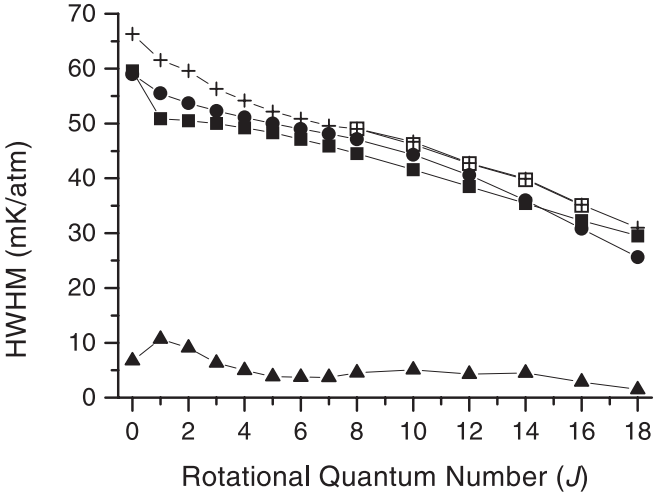

FIGURE 1 Rotational line widths (half-widths at half-maximum) as a function of rotational quantum number. (+) and (□) Experimental rovibrational S_1-branch line widths from [14] and [15, 16], respectively. (■) Rotational line widths approximated from Q-branch line widths [4], using the RPA [10]. (●) Pure rotational S_0 line widths calculated using the semi-classical RB approach (see Sect. 3). (▲) The estimated elastic part of the rovibrational S_1 line widths, cf. (8) (note: $1\ \text{mK} = 10^{-3}\ \text{cm}^{-1}$)

ε (K)	(a)	97.1
σ (Å)	(a)	3.73
d_{ij} (K Å^{12})	(b)	0.268×10^9
e_{ij} (K Å^6)	(b)	0.196×10^6
$\lvert r_{1i}\rvert = \lvert r_{2j}\rvert$ (Å)	(b)	0.55
$Q(10^{-26}$ esu cm$^{-2})$	(c)	–1.4
B_0 (cm^{-1})	(d)	2.0006

TABLE 1 Atomic and molecular parameters for nitrogen. (a) These molecular values result from a fit of a Lennard–Jones 6-12 potential to the isotropic atom–atom potential developed up to the fourth order. (b) [37]. (c) [38], (d) [39]

J	RPA	S_1 [14]	S_1 [15, 16]	RB
0	59.6	66.32 (1.52)		59.0
1	50.9	61.57 (3.50)		55.5
2	50.5	59.60 (1.00)		53.7
3	50.0	56.32 (1.19)		52.3
4	49.2	54.17 (1.27)		51.1
5	48.3	52.14 (1.23)		50.0
6	47.1	50.85 (0.83)		49.0
7	45.9	49.59 (0.94)		48.1
8	44.5	49.04 (0.95)	49.05 (1.00)	47.1
10	41.6	46.67 (0.63)	46.20 (0.19)	44.3
12	38.5	42.78 (0.45)	42.67 (0.78)	40.6
14	35.4	39.90 (0.83)	39.74 (0.06)	36.0
16	32.3	35.18 (0.82)	35.06 (0.70)	30.8
18	29.5	30.99 (1.59)		25.6

TABLE 2 The rotational line widths of Fig. 1 (HWHM in mK atm^{-1})

CARS at room temperature and high pressure is very suitable for such a study.

In order to evaluate the temperature from the rotational CARS spectra, we need information regarding the temperature dependence in the region around 295 K. The temperature dependence of rovibrational Raman line widths of N_2 has recently been studied [15, 16], but only for a few rotational lines and at higher temperatures. Therefore, we have performed semi-classical calculations following the Robert–Bonamy formalism, with the purpose of deriving a temperature-dependence around 295 K for each J-value.

The semi-classical RB formalism has already been used to calculate rotational nitrogen line widths (see [9]), but let us here recall the main features tied to this model. Starting from the Anderson [7] and Tsao–Curnutte [8] theory, called the ATC, the two main improvements are the exponential form of the second-order differential cross section (which avoids the unphysical cut-off procedure of the ATC theory), and the use of a curved trajectory governed by the isotropic potential (instead of the straight line in the ATC model). Within this approach, the line width associated with the optical transition $i \to f$ is written as

$$\gamma_{if} = \frac{n_b}{2\pi c} \sum_{j_2} \varrho_{j_2} \int_0^\infty v f(v) \mathrm{d}v \int_0^\infty 2\pi b \mathrm{d}b \{1 - \exp[-S_2(b, v, 2)]\} \tag{10}$$

where n_b is the number density of perturbing molecules, c is the speed of light, ϱ_{j_2} the population of the j_2 state of the perturber, v the initial relative velocity, $f(v)$ the Maxwell–Boltzmann distribution of velocities and b the impact parameter. The differential cross section $S_2(b, v, 2)$ is expanded to the second order with respect to the intermolecular potential, and it is a function of b, v and of the quantum number of the perturbing molecule (here denoted 2) [9].

The more realistic curved-trajectory model in the RB model requires the inclusion of short-range contributions to the intermolecular potential (contrarily to the ATC). An improved description of the N_2–N_2 potential is obtained by adding an empirical 'atom–atom' potential, $V_{\text{atom–atom}}$, to the electrostatic quadrupole–quadrupole contribution, $V_{Q_1Q_2}$, cf. (11). The parameters d_{ij} and e_{ij} of the 'atom–atom' part have been determined independently from second virial coefficients experiments [37].

$$V = V_{Q_1Q_2} + V_{\text{atom–atom}} = V_{Q_1Q_2} + \sum_{i,j} \left(\frac{d_{ij}}{r_{1i,2j}^{12}} - \frac{e_{ij}}{r_{1i,2j}^{6}} \right). \tag{11}$$

In (11), $r_{1i,2j}$ denotes the distance between the i^{th} atom of molecule 1 and the j^{th} atom of molecule 2. The atom–atom part is then expanded in terms of the distance r between the centres of gravity of the two molecules and of the spherical harmonics tied to the orientations of both molecules in the molecular frame (see Fig. 2). Finally, the intermolecular potential is written as

$$V = 4\pi \sum_{l_1 l_2 m} u_{l_1 l_2 m}(r) Y_{l_1}^m(\theta_1, \varphi_1) Y_{l_2}^{-m}(\theta_2, \varphi_2) \,. \tag{12}$$

The Y_l^m functions are the spherical harmonics and the $u_{l_1 l_2 m}$ functions are the radial functions for the respective order of the spherical harmonics. The expansion has been performed up to the fourth order (powers 10 and 16 of r), and for l_1 and l_2 varying from 0 to 2 (there are only even l_1 and l_2 for homonuclear molecules, or equivalently only even to even or odd to odd transitions are allowed). The $u_{l_1 l_2 m}$ radial components are given in [9].

The pure rotational line-width calculations have been realised using the molecular parameters given in Table 1. In Fig. 1, the line-width values are compared to the RPA approximation and experimental data mentioned above (see also Table 2). It is seen that the RB calculations systematically underestimate the broadening. We therefore propose to use the experimental values at 295 K and to extrapolate these using the temperature dependence given by the RB calculation, which was done in the temperature range 250 to 350 K, by steps of 20 K. The dependence of the calculated broadening coefficients on temperature in this range is linear to a very good approximation; thus we use a linear extrapolation of the experimental values at 295 K:

$$\gamma_{J,J+2}(T) = A(J)(T - 295) + B(J, 295) \tag{13}$$

where the $B(J, 295)$ coefficient is the experimental line width at 295 K (cf. Table 2) and $A(J)$ is the temperature coefficient reported in Table 3. This procedure allows us to build a library of line widths, valid in a region around 295 K, which will be used in the following.

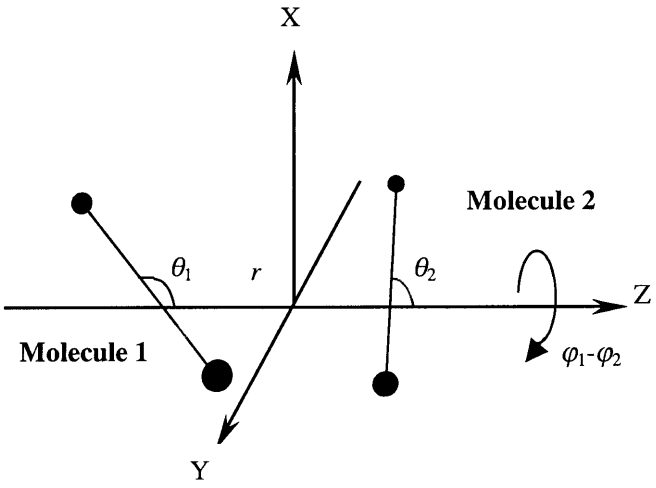

FIGURE 2 Orientation and radial coordinates for two interacting linear molecules. The angles θ_1 and θ_2 are the angles between the molecular axes and the Z axes, and the angle $\varphi_1 - \varphi_2$ is the relative twist of the two molecules about the intermolecular Z-a axis. The intermolecular distance is denoted by r

J	$A(J)$ (10^{-3} cm^{-1}K^{-1}amagat^{-1})
0	0.0393
1	0.0421
2	0.0456
3	0.0477
4	0.0483
5	0.0488
6	0.0497
7	0.0518
8	0.0557
10	0.0669
12	0.0813
14	0.0943
16	0.1038
18	0.1078

TABLE 3 Temperature coefficients $A(J)$ from a linear fit to semi-classically calculated (RB) line widths, cf. (13) (note: γ (10^{-3} cm^{-1}amagat^{-1}) = γ (10^{-3} cm^{-1} atm^{-1})T (K)/273.15)

4 Experimental

The experimental data that we have evaluated has already been presented in [12]. A short summary of the experimental conditions is given below.

The pump beam ω_3 was supplied from a dye laser (using dye Rh610), operated in narrow-band mode (0.2 cm^{-1}), and the two broadband beams, ω_1 and ω_2, from a single dye laser (using dye DCM) with a spectral bandwidth of $\sim$ 120 cm^{-1} centred around 630 nm. The pump laser was tuned to the sodium D_2 line at 589.0 nm and an atomic filter of sodium vapour was used to suppress residual stray light from the pump laser that propagated along the path of the generated CARS signal [40]. The phase-matching scheme was a planar BOXCARS beam configuration, with two broadband beams of equal intensities and one narrow-band beam.

The generated rotational CARS signal was filtered from unwanted radiation originating from the broadband beams and the narrow-band beam by using long-pass dichroic mirrors, apertures, short-pass filters and the already mentioned atomic sodium filter. The signal was then focused onto the entrance slit of a spectrometer and spectrally resolved at the output slit where an unintensified and back-illuminated CCD camera was placed. We measured the resulting instrumental spectral line broadening from the spectrometer/CCD system from nitrogen reference spectra recorded at room temperature and atmospheric pressure. The slit function was found to be purely Gaussian with a full width at half-maximum (FWHM) of 1.45 cm^{-1}. For a more detailed description of the experimental setup, see [12].

The experimental data consist of room-temperature spectra recorded at atmospheric pressure and up to 44 MPa. We have chosen to re-evaluate the spectra below 10 MPa, because in this range the rotational lines are still resolvable and the spectral line fit can be studied. The data consisted of three spectra at each pressure, and each was averaged over 200 laser shots.

The atmospheric pressure spectra were of low quality because of a bad signal-to-noise ratio and because of problems with ASE (amplified spontaneous emission) at high Raman shifts originating from the narrow-band dye laser. Although we used these spectra to fit the instrumental broadening function, the actual values of the temperatures of these spectra are not reliable. At higher pressure the signal-to-noise ratio improved and the problem with ASE decreased to a negligible level.

5 Results and discussion

The temperature evaluation was done with three different models. As reference we used the old CARS code with only anti-Stokes lines included and the RPA line widths (model 1). Further, we evaluated the spectra with a new code including both CARS and CSRS lines using RPA line widths (model 2) and in addition rovibrational S_1 line widths (model 3). We chose to fix the dispersion to an average value of fitted dispersions from spectra at different pressures. The value of the non-resonant susceptibility was fixed to a constant value. Several values of χ_{nr} have been reported in the literature, e.g. $(0.78 \pm 0.18) \times 10^{-17}$ cm^{-3} erg^{-1} atm^{-1} at 298 K [41]. However, we have chosen a value by assuring a good fit at high Raman shifts (above 200 cm^{-1}), where the non-resonant term is more pronounced than the resonant term. The same value could be used for all pressures, but a slightly different value was found for model 1 (0.65×10^{-17} cm^{-3} erg^{-1} atm^{-1} at 298 K) compared to models 2 and 3 (0.60×10^{-17} cm^{-3} erg^{-1} atm^{-1} at 298 K). This is probably due to the influence of the CSRS in the latter models. The parameters that were allowed to vary were the temperature and the Raman shift of the calibration channel.

In Fig. 3, the resulting temperature profiles as a function of pressure are plotted. We can establish that the inclusion of CSRS lines in the spectral calculation increases the temperature by up to 30 K (or 12%), and by at least 5 K (1.5%) over the whole pressure range. With the new rovibrational S_1 line widths the temperature increases slightly more, and the final temperature profile is close to the true temperature up to 7 MPa. Above this pressure the temperature increases, and we have not been able to explain this behaviour with the present model.

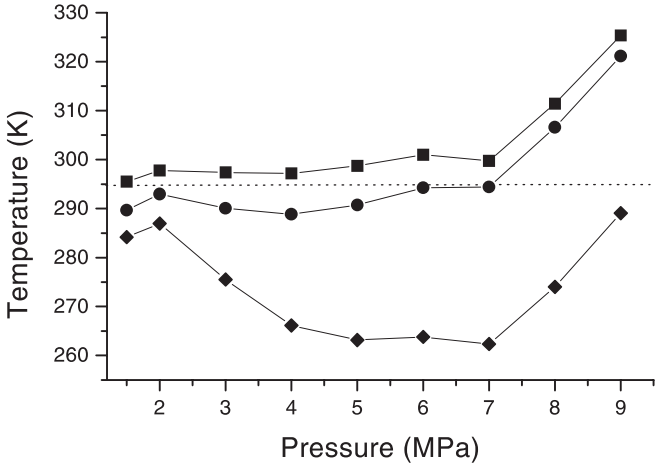

FIGURE 3 Temperature as a function of pressure, evaluated with three different models. (♦) Old model (CARS lines), (●) new model (CARS and CSRS lines) and line widths approximated with the RPA and (■) new model with experimental S_1-branch line widths

In Fig. 4, an experimental spectrum, the best-fitted spectrum and the difference spectrum are plotted at 3.0 and 7.0 MPa, using the three models as explained in relation to Fig. 3. It is evident that the spectral fits are very poor using the old model and that our new model improves the fits significantly, while evaluating a temperature in good agreement with the real value. It should be pointed out that a better fit could be achieved with model 1 if the non-resonant susceptibility was fitted, but the fit was then worse at high Raman shifts where there are no resonant peaks and the temperature was still not affected by more than ~ 3 K.

There is clearly a large influence from the CSRS contribution, even at Raman shifts as high as 50–100 wavenumbers (far from the interfering Stokes lines). Further, the improved spectral fit when using rovibrational line widths, as opposed to line widths approximated from Q-branch line widths, supports the assumption that there is a large re-orientational contribution to the S-branch line widths. However, theoretical calculations of the re-orientational effect indicate a small contribution [34], in fact less than 1 mK atm^{-1} for $J > 2$. Yet, the high-resolution measurements in [14–16] indicate a contribution of 10 mK atm^{-1} and our results support these measurements. Obviously more theoretical and experimental effort is needed on this point.

In the discussion so far, we have neglected the possibility that the experimental conditions could affect the inter-branch interference. We have however noticed that the relative intensities of the CARS and CSRS branches can be altered by changes in the experimental setup, and we believe it might

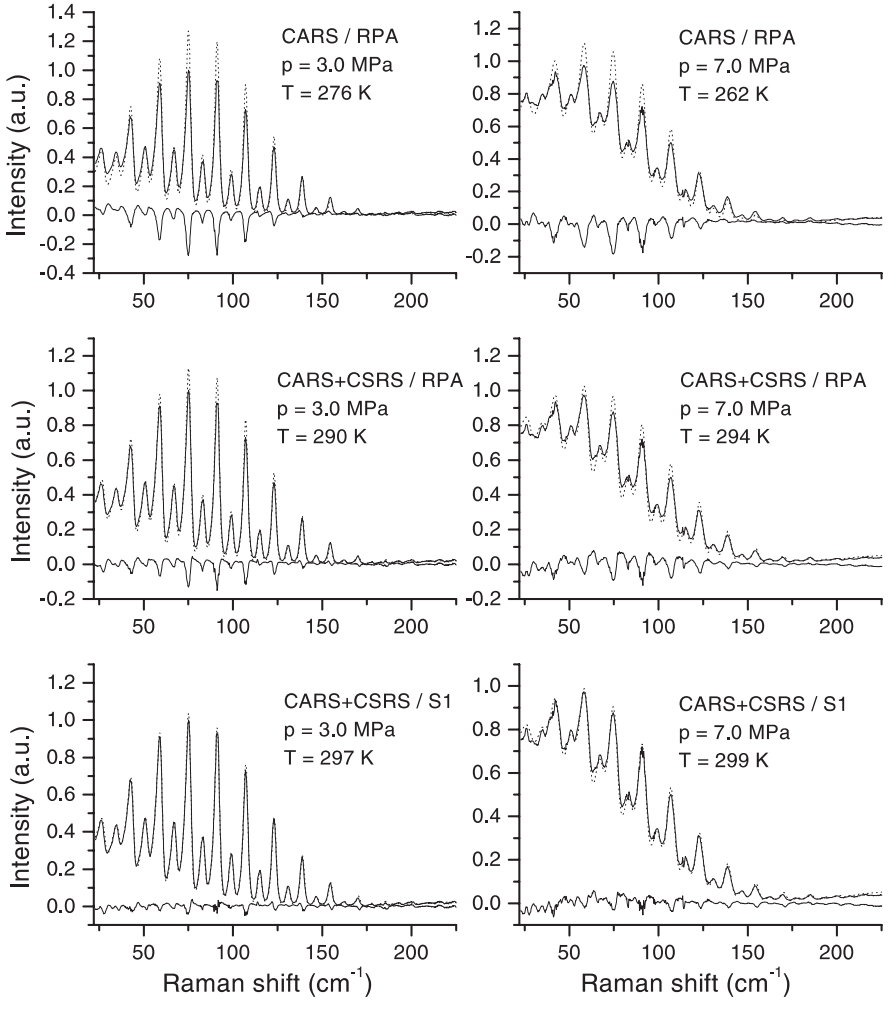

FIGURE 4 Experimental rotational CARS spectra of pure nitrogen (*solid lines*), plotted together with best-fitted theoretical spectra (*dotted lines*) and residual spectra (*bottom solid line*), using the three different models mentioned in Fig. 3 (rows 1, 2, and 3 respectively). The comparison is done at two different pressures, 3.0 and 7.0 MPa (columns 1 and 2, respectively). In each graph the evaluated temperature from the best fits is indicated

be due to the slightly different phase-matching conditions. For example, if there is a spatial dispersion of the signal at a narrow entrance slit of a spectrometer, the inter-branch interference could be affected. In fact, a scaling of the CSRS susceptibility by a factor of ~ 0.8 resulted in a temperature profile closer to 295 K and a slightly better spectral fit. Thus, such possible effects should be kept in mind while designing the experimental setup and during the evaluation of experimental data.

We conclude that a correct modelling of pure rotational CARS spectra at pressures up to 7 MPa and room temperature needs to account for the interference from the CSRS branch and the use of as accurate as possible rotational broadening coefficients. However, at pressures above 7 MPa our model still does not evaluate a correct temperature and the line fit is degrading. Although the reason for the discrepancy is unclear, one may speculate about two different effects, both related to the increasing line overlap with increasing pressure. The first is a narrowing effect similar to that observed in a collapsed vibrational CARS spectrum [42], which is due to the coupling of rotational levels by inelastic collisions. In that case the isolated-line approximation used in this paper does not apply. However, according to Tam and May [43] this effect should not occur for nitrogen until pressures of around 20 MPa. Another potential explanation is related to the spectral signature and the evaluation procedure. It is clear that the temperature evaluation from a rotational CARS spectrum is related to the intensity distribution over the rotational lines. Consequently, when the line character vanishes the temperature sensitivity is less. Thus, for instance, even small systematic errors related to the experiment may influence the evaluated temperature to a larger extent. For example the division of the rotational spectra with a non-resonant spectrum, in order to compensate for the finite bandwidth of the broadband laser, would probably be more critical in this case and the quality of the non-resonant spectra more important. To which extent this can affect the evaluated temperature is unclear.

An interesting question, in the context of rotational CARS thermometry in internal combustion engines, is whether the inter-branch interference needs to be taken into account at such conditions. Our analysis indicates that this effect cannot be neglected when the resonant and non-resonant susceptibilities have the same order of magnitude. That is, when the pressure is high or at moderate pressures and high temperatures. However, in a practical measurement in engines, part of the CARS spectrum at low Raman shifts has to be cut away because of problems with rejection of stray light originating from the pump laser. It is thus not obvious how the interference from CSRS lines would affect such measurements. In the near future, we plan to re-evaluate part of the data from previous engine measurements in order to investigate this issue.

6 Summary

A re-evaluation of temperature from published pure rotational CARS spectra of nitrogen [12] recorded at room temperature and at pressures in the range 1.5–9 MPa has been performed with an improved rotational CARS code. The improvements to the code consist of (i) considering the interference of CSRS (Stokes) lines on the CARS (anti-Stokes) side of the spectrum and (ii) replacing the collision Raman line widths, previously approximated from Q-branch line widths, with more appropriate rovibrational S_1-branch broadening coefficients.

In Paper I [13] the inter-branch interference was described. It is an effect originating from the interaction between the resonant CARS, resonant CSRS and the non-resonant susceptibilities. It has been shown that the inclusion of the CSRS lines in the spectral calculation increases the temperature by up to 30 K (12%) in the range 3–7 MPa, and improves the spectral fit even at large Raman shifts (up to 100 cm^{-1}).

In this paper we have focused on the collision Raman line widths. The pure rotational or rovibrational Raman line widths have a contribution from re-orientation of the molecular axis during the collision, an effect that does not contribute to the isotropic Q-branch. In the absence of pure rotational line-width data, we have used rovibrational S_1-branch line widths, the approximation being reasonable as the vibrational dephasing is negligible. We have shown that the fit between theoretically calculated CARS spectra and experimentally measured ones is improved further with the new line widths, and the evaluated temperature is also improved at pressures up to 7 MPa.

ACKNOWLEDGEMENTS This work is financially supported by the Swedish Research Council. One of the authors (M. Afzelius) wishes to acknowledge The Service Culturel et Scientique of the French Embassy in Sweden and the French Ministry of Foreign Affairs for additional financial support.

REFERENCES

1 D.V. Murphy, R.K. Chang: Opt. Lett. **6**, 233 (1981)
2 B. Dick, A.A. Gierulski: Appl. Phys. B **40**, 1 (1986)
3 L. Martinsson, P.-E. Bengtsson, M. Aldén, S. Kröll: In Temperature, its Measurement and Control in Science and Industry, Vol. 6, ed. by J.F. Schooley (American Institute of Physics, New York 1992) p. 679
4 L. Martinsson, P.-E. Bengtsson, M. Aldén, S. Kröll, J. Bonamy: J. Chem. Phys. **99**, 2466 (1993)
5 L. Martinsson, P.-E. Bengtsson, M. Aldén: Appl. Phys. B **62**, 29 (1996)
6 T. Seeger, A. Leipertz: Appl. Opt. **35**, 2665 (1996)
7 P.W. Anderson: Phys. Rev. **76**, 647 (1949)
8 C.J. Tsao, B. Curnutte: J. Quantum Spectrosc. Radiat. Transfer **2**, 41 (1962)
9 D. Robert, J. Bonamy: J. Phys. Paris **40**, 923 (1979)
10 A.E. DePristo, S.D. Augustin, R. Ramaswamy, H. Rabitz: J. Chem. Phys. **71**, 850 (1979)
11 M.L. Koszykowski, L.A. Rahn, R.E. Palmer, M.E. Coltrin: J. Phys. Chem. **91**, 41 (1987)
12 J. Bood, P.-E. Bengtsson, T. Dreier: J. Raman Spectrosc. **31**, 703 (2000)
13 M. Afzelius, P.-E. Bengtsson: Appl. Phys. B **75**, 763 (2002), DOI 10.1007/s00340-002-1019-0
14 G. Fanjoux, G. Millot, B. Lavorel: J. Raman Spectrosc. **27**, 475 (1996)
15 F. Chaussard, R. Saint-Loup, H. Berger, X. Bruet, P. Joubert, J. Bonamy, D. Robert: In Proc. XXth Eur. CARS Workshop, Lund, Sweden, April 2001
16 F. Chaussard: PhD thesis, Université de Bourgogne, Dijon (2001)
17 M. Aldén, P.-E. Bengtsson, H. Edner: Appl. Opt. **25**, 4493 (1986)
18 A.C. Eckbreth, T.J. Anderson: Opt. Lett. **11**, 496 (1986)
19 M. Aldén, H. Edner, S. Svanberg: Phys. Scr. **27**, 29 (1983)
20 J.B. Zheng, A. Leipertz, J.B. Snow, R.K. Chang: Opt. Lett. **8**, 350 (1983)
21 G. Placzek, E.Z. Teller: Z. Phys. **81**, 209 (1933)
22 T.C. James, W. Klemperer: J. Chem. Phys. **31**, 130 (1959)
23 C. Asawaroengchai, G.M. Rosenblatt: J. Chem. Phys. **72**, 2664 (1980)
24 M.C. Drake, C. Asawaroengchai, G.M. Rosenblatt: ACS Symp. Ser. **134**, 231 (1980)
25 M.C. Drake: Opt. Lett. **7**, 440 (1982)
26 H. Kataoka, S. Maeda, C. Hirose: Appl. Spectrosc. **36**, 565 (1982)

27 R.F. Teets: Opt. Lett. **9**, 226 (1984)
28 B. Lavorel, G. Millot, J. Bonamy, D. Robert: Chem. Phys. **115**, 69 (1987)
29 B. Lavorel, B. Oksengorn, D. Fabre, R. Saint-Loup, H. Berger: Mol. Phys. **75**, 397 (1992)
30 B. Lavorel, G. Millot, R. Saint-Loup, C. Wenger, H. Berger, J.P. Sala, J. Bonamy, D. Robert: J. Phys. Paris **47**, 417 (1986)
31 L.A. Rahn, R.E. Palmer: J. Opt. Soc. Am. B **3**, 1164 (1986)
32 B. Lavorel, L. Guillot, J. Bonamy, D. Robert: Opt. Lett. **20**, 1189 (1995)
33 L. Bonamy, J. Bonamy, D. Robert, B. Lavorel, R. Saint-Loup, R. Chaux, J. Santos, H. Berger: J. Chem. Phys. **89**, 5568 (1988)
34 J.P. Looney, G.J. Rosasco: J. Chem. Phys. **95**, 2379 (1991)
35 J. Buldyreva, J. Bonamy, D. Robert: J. Quantum Spectrosc. Radiat. Transfer **62**, 321 (1999)
36 G.C. Herring, M.J. Dyer, W.K. Bischel: Opt. Lett. **11**, 348 (1986)
37 M. Oobatake, T. Ooi: Prog. Theor. Phys. **48**, 2132 (1972)
38 G. Brocks, A. Van der Avoird: Mol. Phys. **55**, 11 (1985)
39 G. Herzberg: *Molecular Spectra and Molecular Structure* (Van Nostrand, Princeton, New Jersey 1961)
40 J. Bood, P.-E. Bengtsson, M. Aldén: Appl. Opt. **37**, 8392 (1998)
41 R.L. Farrow, R.P. Lucht, L.A. Rahn: J. Opt. Soc. Am. B **4**, 1241 (1987)
42 R.J. Hall, J.F. Verdieck, A.C. Eckbreth: Opt. Commun. **35**, 69 (1980)
43 R.C.H. Tam, A.D. May: Can. J. Phys. **61**, 1558 (1983)